Research Article | Vol. 28, No. 16 / 3 August 2020 / Optics Express 23251
Optics EXPRESS

Laser-induced inner-shell excitations through direct electron re-collision versus indirect collision

YUNPEI DENG,[1] ZHINAN ZENG,[2] PAVEL KOMM,[3] YINGHUI ZHENG,[2] WOLFRAM HELML,[4] XINHUA XIE,[1] ZOLTAN FILUS,[5] MATHIEU DUMERGUE,[5] ROLAND FLENDER,[5] MÁTÉ KURUCZ,[5] LUDOVIT HAIZER,[5] BALINT KISS,[5] SUBHENDU KAHALY,[5] RUXIN LI,[2] AND GILAD MARCUS[3,*]

[1] *SwissFEL, Paul Scherrer Institut, 5232 Villigen PSI, Switzerland*
[2] *State Key Laboratory of High Field Laser Physics, Shanghai Institute of Optics and Fine Mechanics, Chinese Academy of Sciences, Shanghai 201800, China*
[3] *Department of Applied Physics, Faculty of Science, Hebrew University of Jerusalem, Jerusalem 91904, Israel*
[4] *Zentrum für Synchrotronstrahlung, Technische Universität Dortmund, 44227 Dortmund, Germany*
[5] *ELI-ALPS, ELI-HU Non-Profit Ltd., Wolfgang Sandner utca 3, Szeged 6728, Hungary*
[*] *gilad.marcus@mail.huji.ac.il*

Abstract: The dynamics and the decay processes of inner-shell excited atoms are of great interest in physics, chemistry, biology, and technology. The highly excited state decays very quickly through different channels, both radiative and non-radiative. It is therefore a long-standing goal to study such dynamics directly in the time domain. Using few-cycle infrared laser pulses, we investigated the excitation and ionization of inner-shell electrons through laser-induced electron re-collision with the original parent ions and measured the dependence of the emitted x-ray spectra on the intensity and ellipticity of the driving laser. These directly re-colliding electrons can be used as the initiating pump step in pump/probe experiments for studying core-hole dynamics at their natural temporal scale. In our experiment we found that the dependence of the x-ray emission spectrum on the laser intensity and polarization state varies distinctly for the two kinds of atomic systems. Relying on our data and numerical simulations, we explain this behavior by the presence of different excitation mechanisms that are contributing in different ratios to the respective overall x-ray emission yields. Direct re-collision excitation competes with indirect collisions with neighboring atoms by electrons having "drifted away" from the original parent ion.

© 2020 Optical Society of America under the terms of the OSA Open Access Publishing Agreement

Correlations among multiple electrons constitute a corner stone in physics, chemistry, and technology. They are essential processes in various applications of modern technology, including quantum dot lasers [1], quantum logic gates [2], light-harvesting complexes [3], scintillators [4], high harmonic generation (HHG) [5] and entangled-photon sources [6]. In chemistry, electron correlations play an important role in determining molecular structures and for understanding the dynamics of chemical reactions [7]. Electron correlations are inherently at work in atomic relaxation processes such as autoionization, Auger decay and multiple excitation. Multi-electron processes in atoms, such as autoionization and Auger decay, involve a cascaded relaxation through many channels, of which not all necessarily have to be radiative. Pure spectroscopic data, such as line widths and line shapes, may give a rough estimation of the overall time scale of such processes [8]. However, detailed information about the temporal order of these relaxation processes and the coupling between the different states is accessible only through time-domain observations [9–11], in which a first "pump pulse" initiates the process and a second "probe pulse" interrogates

#395927 https://doi.org/10.1364/OE.395927
Journal © 2020 Received 23 Apr 2020; revised 14 Jul 2020; accepted 15 Jul 2020; published 21 Jul 2020

Optics EXPRESS

the system state at a later time. Since the relevant time scale for such dynamics spans from attoseconds to femtoseconds and the relevant energy scale for excitation spans from 10^2 to 10^5 eV, x-ray attosecond bursts may be the choice to serve as the pump and the probe events [12–14]. However, due to the low photon flux of state-of-the-art HHG soft x-ray attosecond sources (for $\hbar\omega$>300 eV) and the low absorption cross sections in this spectral range, it is currently impossible to both pump and probe these processes with such sources. To probe dynamics involving valence electrons, an ultrashort infrared pulse is often used to initiate the process, while the inherently synchronized XUV attosecond pulse probes it [15]. It is difficult to extend this scheme to excite more strongly bound inner-shell electrons, because of the large energy difference between the inner-shell binding energies and the infrared photon energy. Excitation of inner-shell dynamics by laser-induced electron re-collision might be the key to a solution of this experimental challenge.

Here, we present experimental and theoretical results on soft x-ray emission due to laser-induced inner-shell excitation. This work summarizes the collected results from two different laser systems: The first laser has a pulse duration of 12 fs at a central wavelength of 1800nm, a repetition rate of 1 kHz and a pulse energy of up to 0.8 mJ [16]. The second system works with a pulse duration of 60 fs at a central wavelength of 3200 nm, at a repetition rate of 100 kHz and a pulse energy of up to 80 μJ [17]. A schematic drawing of the experiment is shown in Fig. 1. These lasers were focused on a gas jet and we measured the x-ray emission at right angle to the IR beam propagation direction. The 1800nm laser was focused with a 250 mm focal length (f) CaF_2 lens to a spot diameter measured by a knife edge scan to be ~38 μm, while the 3200 nm laser was focused with an effective f = 15 mm parabolic mirror to a spot diameter of ~6 μm. These laser parameters resulted in maximum intensities on target of $\sim 5.8 \times 10^{15}$ W/cm^2 and $\sim 4.5 \times 10^{15}$ W/cm^2, respectively. We estimate an inaccuracy of ~10% for the determination of the focus diameters, thus ~20% inaccuracy in determining the respective intensities. To tune the intensity on target we clipped the beam before the focusing element with an adjustable iris. The gas nozzle was made by drilling a small hole on the side walls of a nickel tube having an outer diameter of 2 mm and wall thickness of 0.1 mm. The gas was fed through one side of the tube while the other side was crimped and welded to force the gas ejection through the drilled orifice. By inspection of the drilled orifice, we estimate its diameter to be ≅100 μm.

In this work we used neon and krypton gas as targets for the inner-shell ionization process, at backing pressures ranging from a few mbar to ~100 mbar. The backing pressure of the neon and krypton gas was measured with a Pirani pressure gauge and/or a differential pressure manometer (PCE-917). At these pressures, and with the above-mentioned dimensions of the orifice, we assume a choked flow through the orifice. The laser was focused as close as possible to the orifice exit, leading to a gas jet diameter at the interaction region of ≅100 μm, with a similar gas density as within the tube. For the x-ray emission detection and spectroscopy, we used a silicon drift detector (Amptek XR-100 SDD) with a 7.6 μm thick beryllium foil as an IR filter in front of it.

In our previous work [18] we used a two-cycle 1800nm laser to excite electrons from inner-shell states of neon and krypton atoms and detected the resulting fluorescence emission from the corresponding K and L transitions. Accompanying the characteristic K and L emission lines, we also observed a continuum x-ray emission, coming from either a bremsstrahlung effect or from recombination radiation. A common practice to separate re-collision related processes, such as high harmonic generation (HHG), from other competing processes is to check the signal against the driving laser polarization ellipticity. As the polarization changes from linear to elliptical, the electrons' trajectories quickly run away from the parent ion and the re-collision related process ceases to exist [19]. Hence, to verify the re-collision mechanism for the case of inner-shell electrons, we checked the fluorescence yield against the laser polarization ellipticity. For that purpose, we placed a quarter waveplate (QWP) just before the focusing element of the IR laser. The ellipticity was calibrated by rotating a linear polarizer after the focus and measuring the transmitted IR power against the polarizer orientation. During our previous work [18] the

Optics EXPRESS

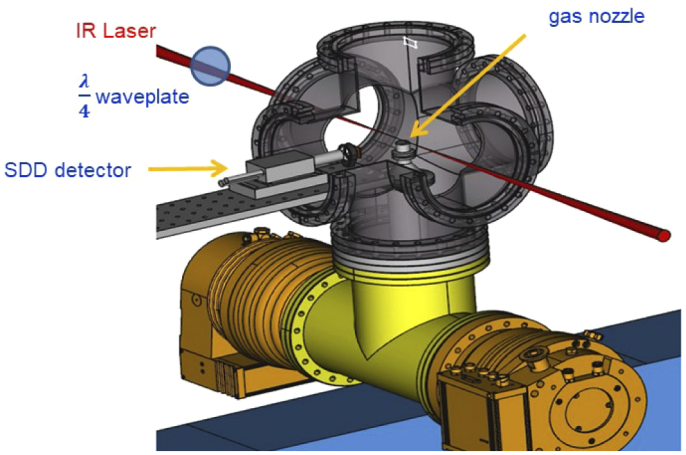

Fig. 1. Schematic drawing of the experiment. A gas nozzle is placed inside a vacuum chamber. The few-cycle IR laser is focused into the gas jet and produces x-ray emission due to electron re-collision and/or electron collision with neighboring atoms. The x-ray yield and spectrum are detected by a silicon drift detector (SDD), which is placed at right angle to the propagation direction of the IR laser beam to avoid the contribution of a possible HHG background. A $\lambda/4$ waveplate is used to control the polarization state of the IR laser on target.

x-ray signal from inner-shell excitation of the Ne atoms was too weak to check the ellipticity dependence, but with krypton we observed a reduction of the x-ray emission correlated with the increase of IR ellipticity. This behavior is a well-known signature of the direct laser-driven electron re-collision process. However, the reduction of the x-ray yield with increasing ellipticity was not as strong as it is usually observed in HHG experiments [19]. In this paper we further investigate these laser-induced inner-shell excitations in more detail and characterize the specific role of electron re-collision.

As a first step, we improved the signal-to-noise ratio and repeated the linear-to-circular polarization scan, for both neon and krypton atoms. Figure 2 shows measured x-ray spectra from neon and krypton as a function of the QWP angle.

The results presented in Fig. 2(b) are similar to those we got in our previous work, i.e. the yield of the characteristic line in krypton peaks at linear polarization and drops to a minimum at circular polarization, though it does not completely disappear. This picture is more detailed than the previous one and we can see a slight shift between the peak position of the characteristic line and the peak position of the continuum. Contrary to Fig. 2(b), Fig. 2(a) shows a completely opposite behavior: both the characteristic K line and the continuum emission from the neon atoms peak around the circular polarization of the IR laser and reduce to a much lower yield near the linear polarization. To explain this, we resort to a competing excitation mechanism. In our first observation of K-shell excitation in neon [12] we concluded that at high gas densities the probability of exciting neighboring atoms by laser-released high-energy electrons is not negligible and has to be considered.

In the following section we would like to elaborate this idea further. We calculate the probabilities for the tunnel-ionized electron to either re-collide with the parent ion and initiate a core-hole excitation, or to drift away from the parent ion and collide with one of the surrounding atoms, again, with high enough kinetic energy to excite a core-shell electron. Hereafter we term these electrons “drift away electrons” (DAWEs). Since our experiments involve many uncertainties such as the exact gas density and the exact laser intensity on target, the goal of the

Optics EXPRESS

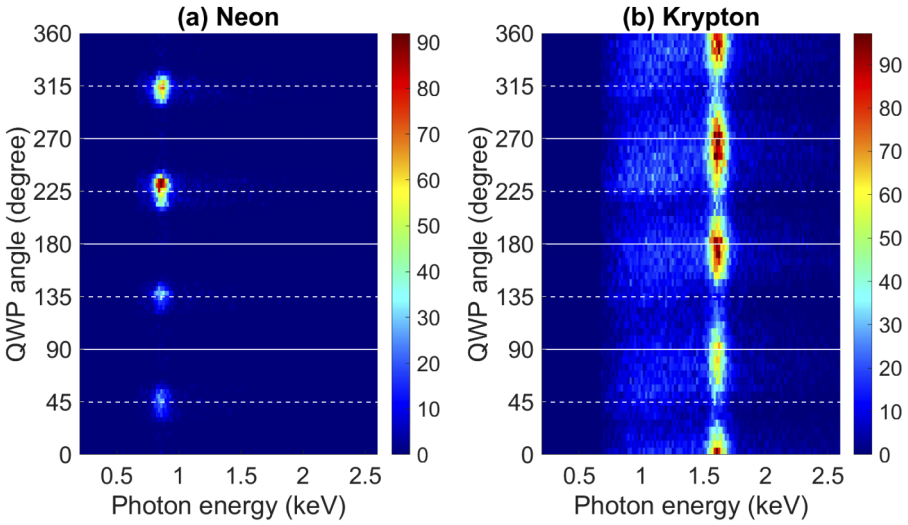

Fig. 2. (a) The x-ray spectrum generated after inner-shell excitation of neon atoms as a function of the QWP angle (linear polarization approximately at 0, 90, 180 & 270 degree, marked as white solid lines; circular polarization at 45, 135, 225 & 315 degree, marked as white dashed lines). The false color map represents number of counts per energy bin. The laser parameters are 1800nm, 12 fs, and 370 μJ (estimated peak intensity on target 2.8×10^{15} W/cm^2). (b) The corresponding x-ray spectrum for krypton atoms as a function of the QWP angle. Same angle markings and laser parameters as (a), except for a pulse energy of 310 μJ (estimated peak intensity 2.3×10^{15}W/cm^2).

following section is to develop a simplified model, which incorporates the essential features of these two excitation mechanisms, and predict within an order of magnitude at which conditions one process dominates over the other. Our model is similar to the famous quasi-classical three-step model [20] that explains most features of HHG qualitatively. As the first step, we assume that a valence electron tunnels out from the atom due to the strong laser field and emerges at the tunnel exit with zero velocity. After tunneling out of the atom, the electron traverses in the strong laser field according to the classical equation of motion. Depending on the time at which the electron has emerged at the tunneling exit, there are two possibilities: the first is that the electron will come back to its parent ion and re-collide with it. The second possibility is that the electron will keep oscillating for more than one period in the laser field with a constant drift velocity that takes the electron away from its parent ion [21]. If the re-colliding electron has enough energy at the collision moment, or the escaping electron has acquired enough energy during its drifting in the laser field, they have a certain probability to "kick" an inner-shell electron from its tightly bound state, while leaving a hole in the inner shell. We would like to compare these two processes of direct re-collision and collision of a DAWE, and calculate the probability ratio between them for different experimental conditions, e.g different laser intensities, laser wavelengths and polarizations, gas densities and different atomic species.

We start by calculating the x-ray fluorescence yield due to direct re-collision. During the excursion of the electron in the continuum, after ionization, the electron wavepacket tends to spread and the overlap between the parent ion core and the ionized electron density reduces. Therefore, we assume that the probability to excite an inner-shell electron due to direct re-collision is proportional to the ratio between the excitation cross section $\sigma(v_r)$ and the electron wavepacket area πw_r^2 at the re-collision time t_r. Thus, the probability per unit time for an electron detached at time $t = t_i$ to excite an inner-shell electron of its parent ion through re-collision at time t_r is

Optics EXPRESS

given by [12,22,23]:

$$dp_{ex}(t_i) = \eta(t_i)\frac{\sigma(v_r)}{\pi w_r^2}dt_i, \tag{1}$$

where $\eta(t_i)$ is the ionization rate at the ionization time t_i and $\sigma(v_r)$ is the excitation cross section as a function of the electron velocity v_r at the re-collision time t_r, and w_r is the electron wavepacket spread at the re-collision time. Note that t_r, v_r and w_r, are all functions of t_i. Note also that the ionization rate depends also on the laser intensity and the ionization potential (see discussion below). The total probability for inner-shell excitation through electron re-collision is the integration of Eq. (1) over the whole pulse duration. Here we neglect re-absorption and assume that the fluorescence yield is proportional to the number of excited atoms in a given volume. The fluorescence yield due to the direct re-collision process is therefore written as:

$$Y_{re} = \rho_0 \Delta V \frac{\Gamma_{rad}}{\Gamma_{Aug}+\Gamma_{rad}} \int \eta(t_i)\frac{\sigma(v_r)}{\pi w_r^2}\, dt_i, \tag{2}$$

where ΔV is the effective volume, defined by the intersection of the focused laser beam and the gas jet, ρ_0 is the gas density, and Γ_{rad} and Γ_{Aug} are the radiative and Auger decay rates, respectively.

To derive the fluorescence yield due to collisions of the DAWEs with neighboring atoms we calculate the respective excitation probabilities as well. For a given electron with a drift velocity v_{drift} the collision probability is $\rho_0\sigma(v_{drift})\Delta L$, where ΔL is the effective distance the electron traverses in the medium. The total probability is therefore the multiplication of this collision probability with the ionization probability, and the fluorescence yield for the collision with neighboring atoms is:

$$\begin{aligned} Y_{DAWE} &= \int \frac{\Gamma_{rad}}{\Gamma_{Aug}+\Gamma_{rad}}[\rho_0\eta(t_i)\Delta V]\rho_0\sigma(v_{drift})\Delta L\, dt_i \\ &= (\rho_0\Delta V)\rho_0\Delta L\frac{\Gamma_{rad}}{\Gamma_{Aug}+\Gamma_{rad}}\int \eta(t_i)\sigma(v_{drift})\, dt_i, \end{aligned} \tag{3}$$

where v_{drift} is the drift velocity of the DAWE which is again a function of the ionization time t_i [20]. Since absolute values are hard to determine, we are most interested in the ratio of these yields. This ratio is given by:

$$\frac{Y_{re}}{Y_{DAWE}} = \frac{1}{\rho_0\Delta L\pi w_r^2}\frac{\int \eta(t_i)\sigma(v_r)\, dt_i}{\int \eta(t_i)\sigma(v_{drift})\, dt_i}, \tag{4}$$

To check the ratios between the fluorescence yields for different experimental conditions we numerically integrate Eq. (4). For the re-collision yield Y_{re} we assumed a linearly polarized laser and calculated $\eta(t_i)$ according to the adiabatic approximation in which the static ionization rate

$$\eta_{stat}(F, I_p, Z) = \omega_0|C_{\chi,l}|^2\left(\frac{2F_0}{F}\right)^{2\xi-1}\exp\left(-\frac{2}{3}\frac{F_0}{F}\right), \tag{5}$$

is now time dependent through the dependency of the electric field *F(t)* on time. (Compare Eq. (4) in [24], where $\hbar = m_e = e = 1$, $\kappa = \sqrt{I_p/13.6\ \mathrm{eV}}$, $\omega_0 = \frac{\kappa^2}{2}$, $F_0 = \kappa^3$, $\xi = Z/\kappa$, Z is the charge state and I_p the respective ionization energy). Because of the long wavelength and therefore low frequency of our laser field, the adiabatic approximation is justified [24–27]. To further simplify our model, we neglected any dependences on angular momentum and magnetic number, thus $|C_{\chi,0}|^2 \cong \frac{2^{2\xi}}{\xi\Gamma(\xi+1)\Gamma(\xi)}$.

With a high enough laser intensity, the probability to release a valence electron reaches unity. At this stage a second electron starts to be tunnel-ionized, with $Z = 2$ and I_p equal to the second

Optics EXPRESS

ionization energy. Once the second electron is ionized a third one starts to be ionized and so on. This process is called sequential multiple ionization. In parallel to the sequential ionization process, there is also a non-sequential ionization process in which the re-colliding electron can ionize another valence electron. The non-sequential ionization is usually dominating at the early stages of ionization, but at higher intensities when the ionization probability comes close to unity, sequential ionization becomes the dominant process [28]. For that reason we consider here only the sequential ionization process. We solve a system of time dependent differential equations:

$$\dot{N}_Z = N_{Z-1}\ \eta(F, I_p(Z), Z) - N_Z\ \eta(F, I_p(Z+1), Z+1), \tag{6}$$

$$\dot{N}_0 = -N_0\ \eta(F, I_p(1), 1),$$

with the initial conditions: $N_Z(t=-\infty) = \begin{cases} 1, & Z=0 \\ 0, & Z\neq 0 \end{cases}$, where N_Z is the Z^{th} charge state population. After solving this system of equations, we have the total ionization rate

$$\eta_{tot}(t) = \sum_Z \dot{N}_Z(t) \tag{7}$$

and we replace $\eta(t_i)$ with $\eta_{tot}(t_i)$ in Eq. (4).

After deriving the ionization rate, we now calculate the re-collision time t_r and the velocity of the electron v_r at the re-collision time by calculating the electron classical trajectories $\vec{r}(t)$ under the influence of the laser field with the assumption of zero velocity at the tunneling time t_i and the requirement that $\vec{r}(t_r) = 0$ [20,29]. For the wavepacket spread w_r we set $w_r(t_i, t_r) = \frac{\hbar}{2m_e w(t_i)}(t_r - t_i)$ [30], and for $\sigma(v)$ we used the Bethe formula $\sigma(v) = A\ E_i\ \ln\left(\frac{m_e v^2}{2E_i}\right) / \left(\frac{1}{2}m_e v^2\right)$ [31–33], where E_i is the binding energy of the inner-shell electron and m_e is the electron mass. Since we are only interested in the ratios between the different fluorescence yields, we can set $A = 1$ (in the case that different channels are involved, we still assume that their cross sections are within the same order of magnitude). For ρ_0 in Eq. (4) we assume similar gas density as within the nickel tube and the effective length ΔL is the gas jet radius at the interaction region (~100 μm). Having $\eta_{tot}(t_i)$, t_r, v_r, $\sigma(v_r)$, w_r, ρ_0 and ΔL, we can plug all these values into Eq. (4).

What remains is to calculate the x-ray fluorescence yield due to the drifting away electrons. We used the Bethe formula for the cross section $\sigma(v)$ as above, but unlike for the re-collision process that occurs mainly at linear IR polarization, with the DAWE we have to distinguish between linear or circular polarization of the driving laser. Hence, in Eqs. (5)–(7) for the ionization rate, we replaced the linearly polarized field $\vec{F}(t) = F(t)\cos(\omega t)\hat{x}$ with the circularly polarized field $\vec{F}(t) = \left(F(t)/\sqrt{2}\right)\ (\cos(\omega t)\hat{x} + \sin(\omega t)\hat{y})$. To understand the main difference in DAWE energy spectra between the linear polarization and circular polarization laser laser field, we have to remember that the DAWE drift velocity, under the assumption of zero velocity at the tunnel exit time t_i, is given by the vector potential at the tunneling time t_i, i.e.:

$$\vec{v}_{drift} = \frac{e}{m_e}\vec{A}(t_i) = \frac{e}{m_e}\int_{t_i}^{\infty} \vec{F}(t)\ dt \tag{8}$$

For the linear polarization, electrons tend to be ionized near the peak of the electric field. According to Eq. (8), for the linear polarization the peak of the electric field is when the magnitude of the vector potential tends to be close to zero. Therefore, the momentum distribution of DAWEs from a linearly polarized driving laser is peaked around zero. The situation for a circularly polarized driving laser is different. In a circularly polarized electric field, the magnitude of the field is constant and only its direction changes in time. In that case, and according to Eq. (8), the vector potential also has a constant magnitude and its direction is always perpendicular to

Optics EXPRESS

the electric field. Thus, with a circularly polarized driver, the DAWE momentum distribution is peaked around this constant value of the vector potential. In addition, with short pulses, we have to account for the change of the electric field amplitude with the pulse envelope, even for the circular polarization case (see Fig. 3).

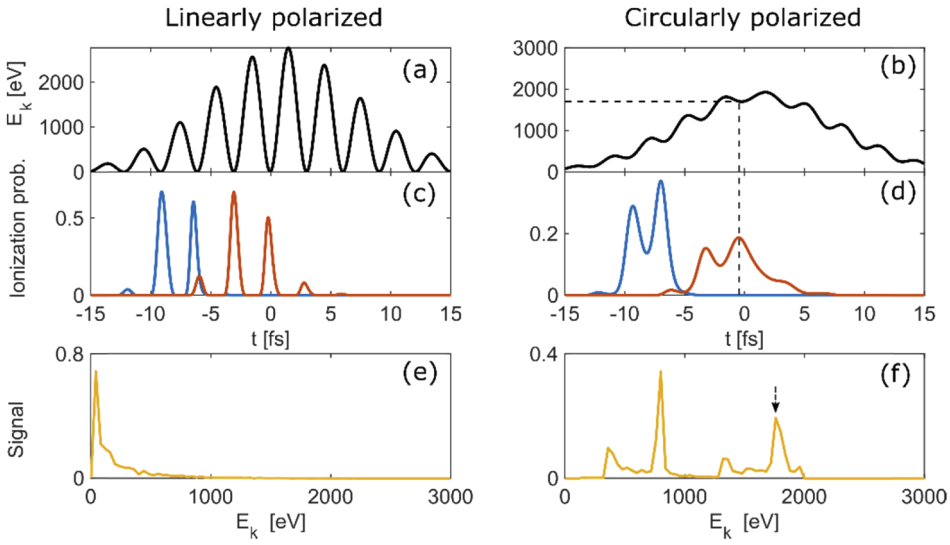

Fig. 3. Calculated DAWE spectra for the linearly and circularly polarized cases. (a) and (b) The kinetic energy of a DAWE which tunnels out at time t for linear polarization and circular polarization, respectively. (c) and (d) The ionization rate of the first and second charge state as a function of time for linear polarization (c) and circular polarization (d) (blue line for $Ne \rightarrow Ne^+$, red line for $Ne^+ \rightarrow Ne^{++}$). (e) and (f) The resulting DAWE energy spectrum for the linear and circular polarization, respectively. In our simulation we used a 1800nm, 12 fs, 6×10^{15} W/cm^2 laser pulse, hence the laser pulse envelope amplitude changes in time for both the linear and the circular polarization cases. The distinct peaks in the electron spectrum for the circular polarization are evidence of multiple ionization (f). The dashed line linking panel (b) and (d) marks the time at which the electrons within the peak in the spectrum around 1800eV (indicated by the dashed arrow) were ionized.

Figure 3 shows typical DAWE spectra for the linear and circular polarization cases. Because of the high intensities in our experiment we also account for multiple ionization. The few distinct peaks in Fig. 3(f) for the circularly polarized driver are the results of multiple ionization. Evidently, in linear polarization, electrons are tending to be ionized at times at which the electric field peaks and the vector potential, as well as the induced electron drift energy, is close to zero. Therefore, the DAWE spectrum is most prominent at low energies. Contrary, the DAWE spectrum generated by the circular laser polarization peaks at higher energies, thus having a higher probability for inner-shell electron excitation.

At this point it is necessary to make some comments on the validity of the above-mentioned model for the high laser intensities used in our experiment. Tunneling through the potential barrier as ionization mechanism is possible as long as the binding energy of the valence electrons is still below the maximum energy of the barrier. For each charge state and its ionization energy there is a threshold laser intensity, beyond which the potential barrier is suppressed sufficiently by the laser electric field that the valence electron can escape even classically. At this point, the ionization mechanism changes from “tunnel ionization” to “barrier suppression ionization” (BSI) with a lower ionization rate. For more details about barrier suppression ionization we refer the reader to [34–36]. Under our experimental conditions at least the first ionization of neon and the

Optics EXPRESS

first three ionization steps of krypton are within the criteria for BSI. Therefore, we simulated electron spectra similar to the ones shown in Figs. 3(e) and (f), but including BSI as in [36]. for comparison (see Fig. 9 in the appendix). The results show only a slight deviation from the ones without the BSI mechanism. In line with our goal to have the simplest model grasping the essential features of our experiment and in the limits imposed by the accuracy of the experimental data, we can neglect this effect in the current discussion. Another issue at such a high laser intensity is whether one needs to include the magnetic field of the laser in the calculations as well. In [28] this question was investigated and it was shown that magnetic field effects can be safely ignored, although minute effects could be observed [37].

Having corroborated the validity of our theoretical model, we use numerical integration to calculate the ratios between the different x-ray emission rates. Figure 4 shows these ratios on a semi-log scale for ionization of neon atoms at different laser intensities. Figure 5 shows the same information for krypton atoms.

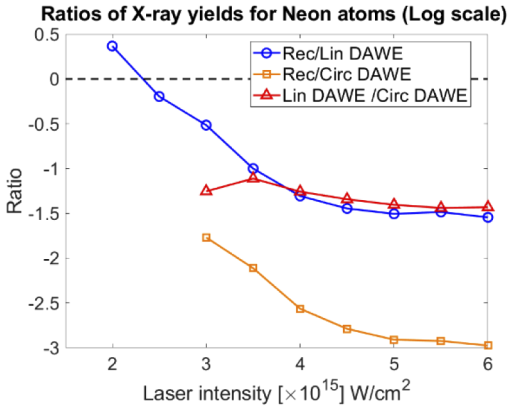

Fig. 4. Results of numerical simulation. Ratios of x-ray yield after ionization in neon as a function of the laser intensity for different excitations mechanisms: "Rec" for re-collision, "Lin DAWE" and "Circ DAWE" for DAWEs from a linearly and circularly polarized laser, respectively. Laser parameters: 12 fs, λ = 1800 nm; gas density ρ_0 = 2.5×10^{18} cm^{-3} and interaction length ΔL = 100 μm. It is evident that at lower laser intensities (I<2.5×10^{15} W/cm^2), and with the given gas density, re-collision excitation dominates over excitation from the linear DAWE mechanism. At higher laser intensities, both the signals from linear DAWEs and from circular DAWEs overcome the re-collision-induced x-ray emission.

Figures 6(a) and (b) shows the measured x-ray emission spectra after ionization of krypton atoms at two different laser intensities in a false color plot as a function of the QWP angle. Both measurements were done with 60 fs laser pulse duration at a driving wavelength of 3200 nm at an estimated laser intensity of 1.1×10^{15} W/cm^2 for Fig. 6(a) and 2.3×10^{15} W/cm^2 for Fig. 6(b). Figure 6(b) presents a similar shape of the fluorescence yield as a function of the laser polarization ellipticity as the shape presented in Fig. 2(a) for ionization in neon atoms, driven by the 1800nm laser at comparable intensities, but different from the shape of the fluorescence yield for ionization of the krypton atoms at 1800nm laser wavelength shown in Fig. 2(b). The main experimental difference between the two cases is the higher ponderomotive energy for the longer-wavelength driving laser used for the data in Fig. 6(b). For the data shown in Fig. 6(a), we reduced the ponderomotive energy and indeed see a shift of the maximum x-ray yield from circularly polarized light towards some more elliptical polarization, but the shift towards linear polarization, as it appears in Fig. 2(b) is not fully recovered.

Optics EXPRESS

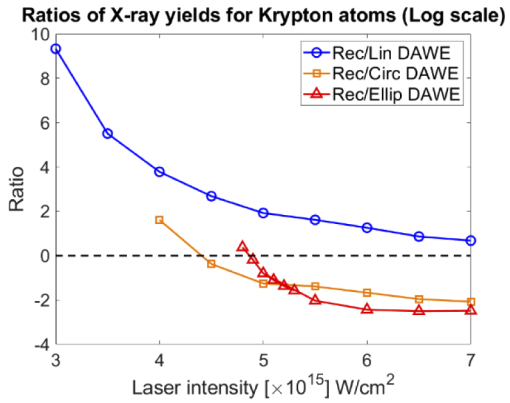

Fig. 5. Same as Fig. 4, but shows the ratios of x-ray yield after ionization of krypton atoms. It is evident that for krypton with the given gas density, re-collision excitation dominates over excitation from linear DAWEs over the whole simulated laser intensity range. For intensities above 4.5×10^{15} W/cm^2, excitation by DAWEs from a circularly polarized laser becomes dominant over re-collision excitation, and above 5.0×10^{15} W/cm^2 also excitation by DAWEs from an elliptically polarized laser ($\varepsilon = 0.7$). These results are in par with the experimental results (see below and Fig. 8).

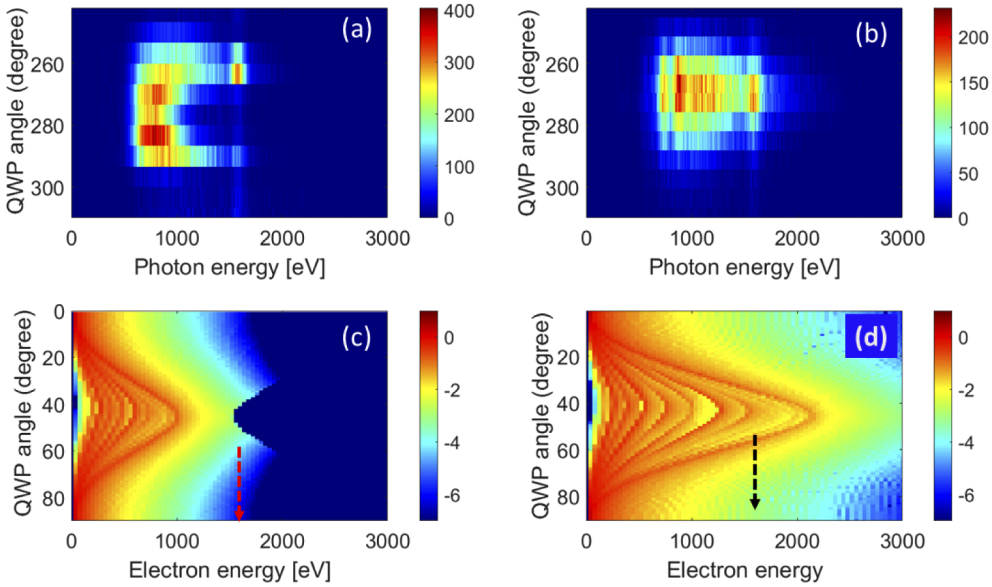

Fig. 6. (a,b) Experimental data: x-ray spectra after ionization in krypton as a function of QWP angle, where 230° corresponds to linear polarization and 275° to circular polarization. Laser parameters: $\lambda = 3200$ nm, $\tau_p = 60$ fs. The estimated laser intensity for the data in (a) is 1.1×10^{15} W/cm^2 and 2.3×10^{15} W/cm^2 for the data in (b). (c,d) Numerical calculation of the DAWEs energy spectrum as a function of the QWP angle (0° corresponds to linear laser polarization and 45° to circular polarization in this calculation) for the same laser parameters as in (a) and (b), respectively. The red and black arrows indicate the energy of the krypton L-shell (1590 eV).

Optics EXPRESS

To understand this trend better, we investigate the corresponding DAWE spectrum. For a given laser intensity, the peak field in a circularly polarized laser is $\sqrt{2}$ times smaller than the peak field of a linearly polarized laser pulse. Therefore, below a certain laser intensity threshold, the kinetic energy of the DAWE driven by a circular polarization pulse does not suffice to excite inner-shell electrons, while at the same intensity for linear polarization the DAWE energy will suffice. In such a case, DAWEs from a linearly polarized laser are more probable to excite inner-shell electrons than DAWEs from a circularly polarized laser, although, on average, DAWEs from a circularly polarized laser have higher energies than those driven by a linearly polarized laser. Taking the two effects together, it can happen that at certain intensities the maximum probability for inner-shell excitation occurs at some ellipticity $0<\varepsilon<1$. Figures 6(c) and (d) shows the simulated DAWE energy spectra on a false color logarithmic scale as a function of the QWP angle, for the same laser parameters as in the experiment. At the lower laser intensities in Fig. 6(a)), we can attribute the dip in the L-shell x-ray emission, around the circular polarization setting, to the similar dip in the electron energy spectrum (Fig. 6(c)). At higher laser intensities, this dip disappears for both the x-ray emission and the electron energy spectrum (Figs. 6(b) and 6(d)). Figure 6 demonstrates the importance of the laser intensity for the ratio of the fluorescence yields at linear or circular laser polarization.

To study this effect further we checked this ratio for a range of intensities. Figure 7(a) shows experimental data, how the characteristic x-ray yield from ionized neon atoms changes as a function of the laser peak intensity, for the linear and circular laser polarization with $\lambda_0 = 3200$ nm and a pulse duration of 60 fs. Figure 7(b) shows the ratio between these x-ray yields on a semi-log scale, and Fig. 7(c) presents our corresponding numerical calculation of the yield ratios on a semi-log scale.

By comparing the experimental results and our numerical calculation we see that at a low intensity, and for a given gas density, the re-collision excitation dominates over excitation by DAWEs for the linear laser polarization. However, at higher intensities inner-shell excitation by DAWEs takes over. This general trend also shows up in the set of data that was taken for ionization of krypton atoms exposed to laser pulses with 12 fs pulse duration and a wavelength $\lambda = 1800$nm. Figure 8 presents false color plots for the x-ray emission spectra from ionized krypton as a function of the QWP at three different laser intensities. At low intensities (panel 8(c)), it shows preferable excitation with linear laser polarization for both the Kr characteristic line and for the surrounding continuum. As the laser intensity increases (8(b)), the peak emission of the continuum shifts towards the circular laser polarization state, and at the highest intensity (Fig. 8(a)) we see higher more characteristic x-ray at the circularly polarization laser state. This is in accordance with our numerical simulations (see above).

In conclusion, while the mechanism of laser-induced electron re-collision remains the same for HHG and for electron impact ionization/excitation of valence electrons, the extension towards keV energies and interactions with inner-shell electrons is not trivial. Several factors are involved in these differences: first, because of the high ponderomotive potential needed to reach inner-shell electrons, the atom experiences a series of sequential tunnel ionization events towards a higher ionization state, as opposed to "low energy" HHG (< 100 eV), where we usually have a single ionization state. Second, since the inner-shell electrons are closer to the atom nuclei and partially screened by the valence electrons, their interaction cross section with the fast re-colliding electron is significantly smaller than the recombination cross section of the slower electrons with the parent ion that usually happens in the "low energy" HHG. As a result, other competing processes are brought to the front of the stage which make it more difficult to study the inner-shell excitations. One of the main competing processes is electron collision with neighboring atoms. Despite some earlier evidence [12,18], the possibility to ionize/excite inner-shell electrons by laser-induced electron re-collision remained controversial. The goal of this research is to improve our knowledge about inner-shell excitation through laser-induced re-collision.

Optics EXPRESS

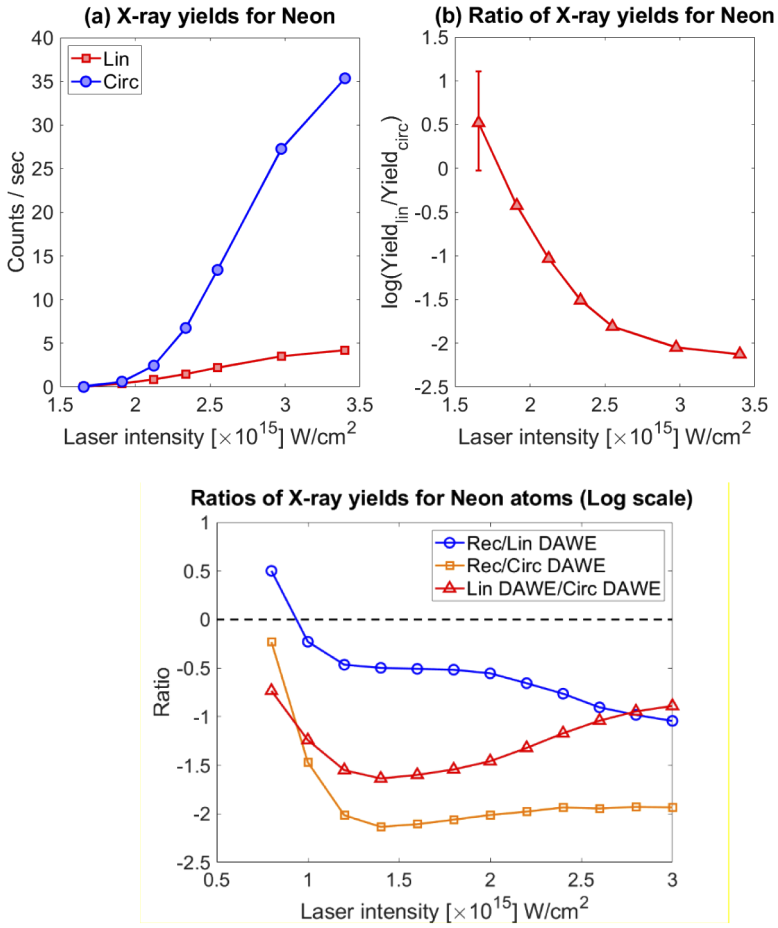

Fig. 7. (a) Experimental data: Ne characteristic x-ray line yield as a function of the drive laser intensity, for both linear and circular polarizations. (b) The ratio between linear polarization yield and circular polarization yield on a semi-log scale. Error bars are too small to be shown except for the first point in (b), where the number of counts is small. (c) Numerical simulation: Ratios of x-ray yields after ionization of neon as a function of excitation mechanism. Rec for direct electron re-collision, Lin DAWE and Circ DAWE for DAWEs generated by a linearly and circularly polarized laser, respectively. Parameters for all panels: $\tau_p = 60$ fs, $\lambda = 3200$ nm; gas density $\rho_0 = 2.5 \times 10^{18}$ cm^{-3}; interaction length $\Delta L = 100$ μm.

Optics EXPRESS

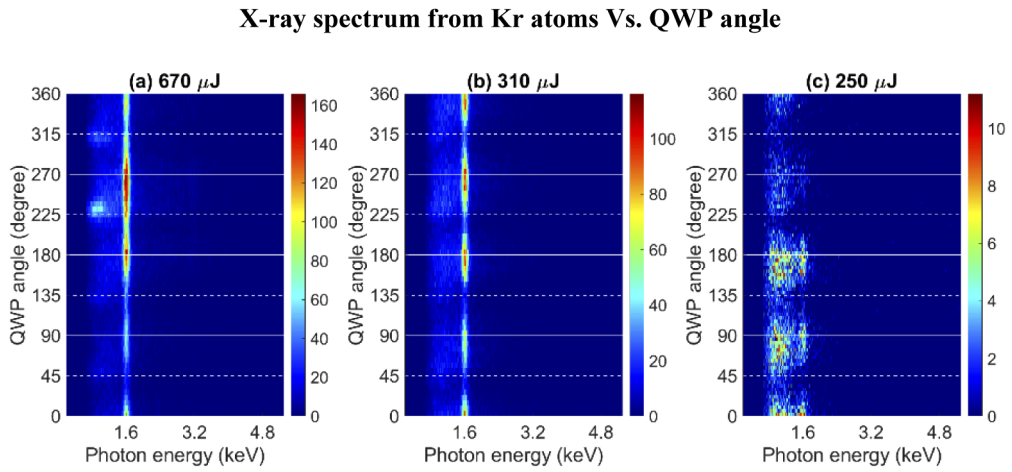

Fig. 8. False color plots of x-ray emission spectra after ionization of krypton atoms at different laser intensities and for different polarization states. The vertical scale shows the QWP angle. White solid horizontal lines mark the approximate linear polarization, while dashed white lines mark approximately the circular polarization. Laser parameters: $\lambda = 1800\ nm$, pulse duration 12 fs. The estimated laser intensities are (a) 5.1×10^{15} W/cm^2, (b) 2.3×10^{15} W/cm^2, and (c) 2.0×10^{15} W/cm^2.

In view of the possibility to use the re-collision process as the initiating process in a pump/probe experiment for studying core-hole dynamics, we examined the conditions under which direct electron re-collision excitation of K-shell and L-shell electrons in neon and krypton, respectively, are dominating over excitation by DAWEs. We measured the x-ray emission perpendicular to the propagation direction of the incoming infrared laser and observed both the K-shell and L-shell characteristic lines, as well as a continuum emission, which we attribute to bremsstrahlung or recombination processes. To verify the re-collision mechanism for the case of inner-shell electrons, we checked the fluorescence yield against the laser polarization ellipticity. We found that at low laser intensities it peaks at linear polarization but observed a shift of the maximum fluorescence yield towards circular polarization for higher laser intensities. According to our calculations, we explain this behavior by the domination of the indirect collision-induced ionization mechanism with neighboring atoms for laser intensities above an element-specific intensity threshold. These results are an important step towards the possibility to use IR-field driven electron re-collision as the initiating pump step in pump/probe experiments for studying core-hole dynamics at their natural temporal scale. We believe that this work can also shed some light on challenges experienced in earlier attempts to generate HH radiation beyond the keV spectral range.

Appendix

Figure 9 shows the effect of BSI compared to tunnel ionization for the same laser conditions as in Fig. 3 with Ne atoms as target. For the calculation of the BSI rate we used the formula from [36] with $\alpha = 12$.

Optics EXPRESS

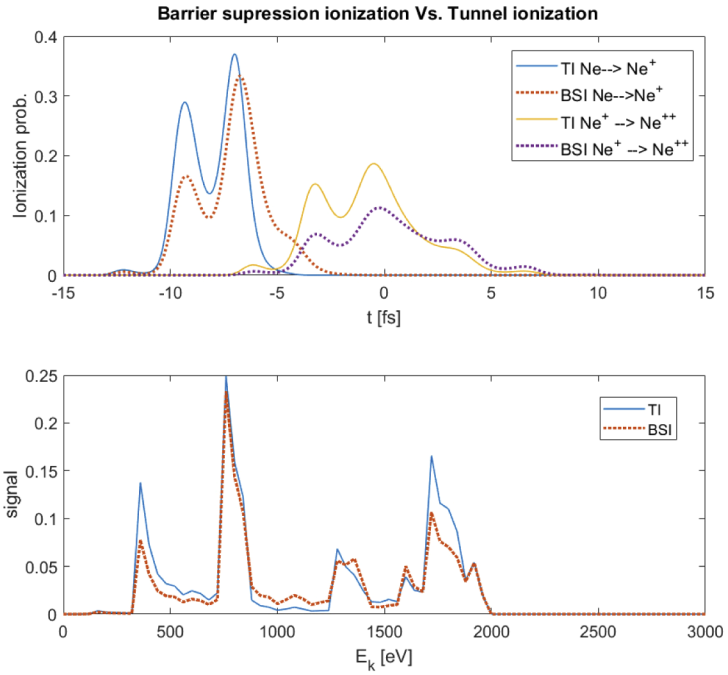

Fig. 9. Simulation of BSI compared to tunnel ionization at the same laser conditions as in Fig. 3 for the first two ionization steps in Ne atoms. TI – tunnel ionization. BSI – Barrier Suppression Ionization.

Funding

Wolfson Foundation; European Regional Development Fund (GINOP-2.3.6-15-2015-00001); European Cooperation in Science and Technology (CA17126(TUMIEE)).

Disclosures

The authors declare no conflicts of interest

References

1. V. I. Klimov, A. A. Mikhailovsky, S. Xu, A. Malko, J. A. Hollingsworth, C. A. Leatherdale, H.-J. Eisler, and M. G. Bawendi, "Optical Gain and Stimulated Emission in Nanocrystal Quantum Dots," Science **290**(5490), 314–317 (2000).
2. X. Li, Y. Wu, D. Steel, D. Gammon, T. H. Stievater, D. S. Katzer, D. Park, C. Piermarocchi, and L. J. Sham, "An All-Optical Quantum Gate in a Semiconductor Quantum Dot," Science **301**(5634), 809–811 (2003).
3. D. Abramavicius, D. V. Voronine, and S. Mukamel, "Double-quantum resonances and exciton-scattering in coherent 2D spectroscopy of photosynthetic complexes," Proc. Natl. Acad. Sci. U. S. A. **105**(25), 8525–8530 (2008).
4. M. Kirm, V. Nagirnyi, E. Feldbach, M. De Grazia, B. Carré, H. Merdji, S. Guizard, G. Geoffroy, J. Gaudin, N. Fedorov, P. Martin, A. Vasil'ev, and A. Belsky, "Exciton-exciton interactions in CdWO_{4} irradiated by intense femtosecond vacuum ultraviolet pulses," Phys. Rev. B **79**(23), 233103 (2009).
5. S. Sukiasyan, C. McDonald, C. Destefani, M. Yu. Ivanov, and T. Brabec, "Multielectron Correlation in High-Harmonic Generation: A 2D Model Analysis," Phys. Rev. Lett. **102**(22), 223002 (2009).
6. R. M. Stevenson, R. J. Young, P. Atkinson, K. Cooper, D. A. Ritchie, and A. J. Shields, "A semiconductor source of triggered entangled photon pairs," Nature **439**(7073), 179–182 (2006).
7. K. Raghavachari and J. B. Anderson, "Electron Correlation Effects in Molecules," J. Phys. Chem. **100**(31), 12960–12973 (1996).
8. M. Jurvansuu, A. Kivimäki, and S. Aksela, "Inherent lifetime widths of Ar $2p^{-1}$, Kr $3d^{-1}$, Xe $3d^{-1}$, and Xe $4d^{-1}$ states," Phys. Rev. A **64**(1), 012502 (2001).

Optics EXPRESS

9. T. Uphues, M. Schultze, M. F. Kling, M. Uiberacker, S. Hendel, U. Heinzmann, N. M. Kabachnik, and M. Drescher, "Ion-charge-state chronoscopy of cascaded atomic Auger decay," New J. Phys. **10**(2), 025009 (2008).
10. A. J. Verhoef, A. V. Mitrofanov, X. T. Nguyen, M. Krikunova, S. Fritzsche, N. M. Kabachnik, M. Drescher, and A. Baltuška, "Time-and-energy-resolved measurement of Auger cascades following Kr 3d excitation by attosecond pulses," New J. Phys. **13**(11), 113003 (2011).
11. F. Penent, J. Palaudoux, P. Lablanquie, L. Andric, R. Feifel, and J. H. D. Eland, "Multielectron Spectroscopy: The Xenon 4d Hole Double Auger Decay," Phys. Rev. Lett. **95**(8), 083002 (2005).
12. G. Marcus, W. Helml, X. Gu, Y. Deng, R. Hartmann, T. Kobayashi, L. Strueder, R. Kienberger, and F. Krausz, "Subfemtosecond K-Shell Excitation with a Few-Cycle Infrared Laser Field," Phys. Rev. Lett. **108**(2), 023201 (2012).
13. T. Popmintchev, M.-C. Chen, D. Popmintchev, P. Arpin, S. Brown, S. Ališauskas, G. Andriukaitis, T. Balčiunas, O. D. Mücke, A. Pugzlys, A. Baltuška, B. Shim, S. E. Schrauth, A. Gaeta, C. Hernández-García, L. Plaja, A. Becker, A. Jaron-Becker, M. M. Murnane, and H. C. Kapteyn, "Bright Coherent Ultrahigh Harmonics in the keV X-ray Regime from Mid-Infrared Femtosecond Lasers," Science **336**(6086), 1287–1291 (2012).
14. S. M. Teichmann, F. Silva, S. L. Cousin, M. Hemmer, and J. Biegert, "0.5-keV Soft X-ray attosecond continua," Nat. Commun. **7**(1), 11493 (2016).
15. F. Krausz and M. Ivanov, "Attosecond physics," Rev. Mod. Phys. **81**(1), 163–234 (2009).
16. C. Zhang, P. Wei, Y. Huang, Y. Leng, Y. Zheng, Z. Zeng, R. Li, and Z. Xu, "Tunable phase-stabilized infrared optical parametric amplifier for high-order harmonic generation," Opt. Lett. **34**(18), 2730–2732 (2009).
17. S. Kühn, M. Dumergue, S. Kahaly, S. Mondal, M. Füle, T. Csizmadia, B. Farkas, B. Major, Z. Várallyay, E. Cormier, M. Kalashnikov, F. Calegari, M. Devetta, F. Frassetto, E. Månansson, L. Poletto, S. Stagira, C. Vozzi, M. Nisoli, P. Rudawski, S. Maclot, F. Campi, H. Wikmark, C. L. Arnold, C. M. Heyl, P. Johnsson, A. L'Huillier, R. Lopez-Martens, S. Haessler, M. Bocoum, F. Boehle, A. Vernier, G. Iaquaniello, E. Skantzakis, N. Papadakis, C. Kalpouzos, P. Tzallas, F. Lépine, D. Charalambidis, K. Varjú, K. Osvay, and G. Sansone, "The ELI-ALPS facility: the next generation of attosecond sources," J. Phys. B: At., Mol. Opt. Phys. **50**(13), 132002 (2017).
18. Y. Deng, Z. Zeng, Z. Jia, P. Komm, Y. Zheng, X. Ge, R. Li, and G. Marcus, "Ultrafast Excitation of an Inner-Shell Electron by Laser-Induced Electron Recollision," Phys. Rev. Lett. **116**(7), 073901 (2016).
19. K. S. Budil, P. Salieres, M. D. Perry, and A. L'Huillier, "Influence of ellipticity on harmonic generation," Phys. Rev. A **48**(5), R3437–R3440 (1993).
20. P. B. Corkum, "Plasma perspective on strong field multiphoton ionization," Phys. Rev. Lett. **71**(13), 1994–1997 (1993).
21. M. Kahn and G. Marcus, "Proposal for strong field physics simulation by means of optical waveguide," J. Phys. B: At., Mol. Opt. Phys. **50**(9), 095004 (2017).
22. P. Colosimo, G. Doumy, C. I. Blaga, J. Wheeler, C. Hauri, F. Catoire, J. Tate, R. Chirla, A. M. March, G. G. Paulus, H. G. Muller, P. Agostini, and L. F. DiMauro, "Scaling strong-field interactions towards the classical limit," Nat. Phys. **4**(5), 386–389 (2008).
23. J. Tate, T. Auguste, H. G. Muller, P. Salieres, P. Agostini, and L. F. DiMauro, "Scaling of Wave-Packet Dynamics in an Intense Midinfrared Field," Phys. Rev. Lett. **98**(1), 013901 (2007).
24. A. M. Perelomov, V. S. Popov, and M. V. Terent'ev, "Ionization of Atoms in an Alternating Electric Field," Sov. Phys. JETP **23**, 924 (1966).
25. A. M. Perelomov and V. S. Popov, "Ionization of Atoms in an Alternating Electrical Field. Ill," Sov. Phys. JETP **25**, 336 (1967).
26. Y. H. Lai, J. Xu, U. B. Szafruga, B. K. Talbert, X. Gong, K. Zhang, H. Fuest, M. F. Kling, C. I. Blaga, P. Agostini, and L. F. DiMauro, "Experimental investigation of strong-field-ionization theories for laser fields from visible to midinfrared frequencies," Phys. Rev. A **96**(6), 063417 (2017).
27. V. S. Popov, "Tunnel and multiphoton ionization of atoms and ions in a strong laser field (Keldysh theory)," Phys.-Usp. **47**(9), 855–885 (2004).
28. S. Palaniyappan, A. DiChiara, E. Chowdhury, A. Falkowski, G. Ongadi, E. L. Huskins, and B. C. Walker, "Ultrastrong Field Ionization of Ne^{n+} ($n \leq 8$): Rescattering and the Role of the Magnetic Field," Phys. Rev. Lett. **94**(24), 243003 (2005).
29. M. Lewenstein, Ph. Balcou, M. Yu. Ivanov, A. L'Huillier, and P. B. Corkum, "Theory of high-harmonic generation by low-frequency laser fields," Phys. Rev. A **49**(3), 2117–2132 (1994).
30. J. J. Sakurai, Modern Quantum Mechanics (Addison-Wesley, n.d.).
31. V. M. Pessa and W. R. Newell, "Electron Impact Ionization Cross Sections of Inner Atomic Shells," Phys. Scr. **3**(3-4), 165–168 (1971).
32. G. Laricchia, P. Van Reeth, S. E. Fayer, S. J. Brawley, R. Kadokura, A. Loreti, and M. Shipman, "A statistical description of scattering at the quantum level," Sci. Rep. **8**(1), 15056 (2018).
33. T. Takayanagi, "Subshell and innershell excitation in rare gas atoms by electron impact," AIP Conf. Proc. **295**, 326–335 (1993).
34. S. Augst, D. D. Meyerhofer, D. Strickland, and S. L. Chin, "Laser ionization of noble gases by Coulomb-barrier suppression," J. Opt. Soc. Am. B **8**(4), 858–867 (1991).
35. V. P. Krainov, "Ionization rates and energy and angular distributions at the barrier-suppression ionization of complex atoms and atomic ions," J. Opt. Soc. Am. B **14**(2), 425–431 (1997).

Optics EXPRESS

36. X. M. Tong and C. D. Lin, "Empirical formula for static field ionization rates of atoms and molecules by lasers in the barrier-suppression regime," J. Phys. B: At., Mol. Opt. Phys. **38**(15), 2593–2600 (2005).
37. B. Willenberg, J. Maurer, B. W. Mayer, and U. Keller, "Sub-cycle time resolution of multi-photon momentum transfer in strong-field ionization," Nat. Commun. **10**(1), 5548 (2019).

132.64.56.238 {ts '2020-07-22 04:05:20'}